Available online at www.sciencedirect.com

ScienceDirect

International Journal of Solids and Structures 44 (2007) 6826–6841

INTERNATIONAL JOURNAL OF SOLIDS AND STRUCTURES

www.elsevier.com/locate/ijsolstr

A continuum approach to the analysis of the stress field in a fiber reinforced composite with a transverse crack

Michael Ryvkin *, Jacob Aboudi

Department of Solid Mechanics, Materials and Systems, Faculty of Engineering, Tel Aviv University, Ramat Aviv 69978, Israel

Received 31 December 2006; received in revised form 12 March 2007
Available online 19 March 2007

Abstract

The stress field in a periodically layered composite with an embedded crack oriented in the normal direction to the layering and subjected to a tensile far-field loading is obtained based on the continuum equations of elasticity. This geometry models the 2D problem of fiber reinforced materials with a transverse crack. The analysis is based on the combination of the representative cell method and the higher-order theory. The representative cell method is employed for the construction of Green's functions for the displacements jumps along the crack line. The problem of the infinite domain is reduced, in conjunction with the discrete Fourier transform, to a finite domain (representative cell) on which the Born–von Karman type boundary conditions are applied. In the framework of the higher-order theory, the transformed elastic field is determined by a second-order expansion of the displacement vector in terms of local coordinates, in conjunction with the equilibrium equations and these boundary conditions. The accuracy of the proposed approach is verified by a comparison with the analytical solution for a crack embedded in a homogeneous plane.

Results show the effects of crack lengths, fiber volume fractions, ratios of fiber to matrix Young's moduli and matrix Poisson's ratio on the resulting elastic field at various locations of interest. Comparisons with the predictions obtained from the shear lag theory are presented.

Keywords: Periodic composites; Representative cell method; Higher-order theory; Broken fibers; Cracked composites

1. Introduction

The problem of cracked fiber reinforced materials received considerable attention. The analysis of this problem is complicated due to the existence of the crack and the surrounding fiber and matrix constituents that give rise to sharp stress gradients. The conventional homogenization approach in which the fiber reinforced material is replaced by an equivalent homogeneous anisotropic medium with am embedded crack is not applicable since it cannot provide the exact stress distribution in the individual fiber and matrix phases close to the crack (which is the region of interest).

* Corresponding author. Tel.: +972 3 6408130; fax: +972 3 6407617.
E-mail address: arikr@eng.tau.ac.il (M. Ryvkin).

0020-7683/$ - see front matter
doi:10.1016/j.ijsolstr.2007.03.011

A possible approach to analyze the problem of cracked composites is the direct modeling of the material microstructure by finite element method. This requires the modeling of the region that consists of the crack and its surrounding fiber and matrix phases by large number of degrees of freedom. Consequently, the size of the finite element grid that models this region is limited. Such an approach was employed by Reedy (1984) who developed a three-dimensional finite element procedure for a monolayer with several fibers one of which is broken. Alternatively, it is possible to increase the size of the finite element model by replacing the fiber and matrix phases located at a sufficiently remote distance from the region of interest by a finite portion of an equivalent anisotropic material. This approach was followed by Nedele and Wisnom (1994) who considered a three-dimensional problem in which the composite material region of fine modeling consists of six fibers surrounding a broken one.

The shear lag approximation was extensively employed to analyze the problem of a transverse crack embedded in a fiber reinforced martial that is subjected to a far-field tensile loading. Contrary to the direct finite element approach, this method enables the modeling of the cracked composite that extends over an infinite domain. The shear lag analysis provides a good approximation of the average stresses in the fiber and matrix regions in the case of a sufficiently large contrasts between the fiber/matrix elastic moduli. This method was employed by Hedgepeth (1961), Hedgepeth and Van Dyke (1967), Dharani et al. (1983), Hikiami and Chou (1990), Sastry and Phoenix (1993) and Beyerlin et al. (1996) for example. One of the limitations of the classical shear lag method is the neglect of the axial stress in the matrix. An improved shear lag analysis was presented by Ochai et al. (1991), Beyerlein and Landis (1999) and Landis and McMeeking (1999) for example, where the axial stiffness of the matrix was taken into account. An extensive literature review of many papers which employ the shear lag approach for the analysis of cracked composites was presented by Beyerlein and Landis (1999).

In the present paper, an exact micromechanical analysis which is based on the elasticity theory is offered for the prediction of the elastic field in a cracked fiber reinforced composite that is subjected to an arbitrary remote loading. The present approach is capable to model the composite with infinite number of distinct fibers without the simplifying assumptions of the shear lag theory. This approach models the cracked unidirectional fiber reinforced material in the framework of a two-dimensional layout that consists of periodically alternating layers which represent the fiber and matrix phases with an embedded crack oriented normal to the layering. The crack problem is represented by a superposition of unit normal displacement jump solutions everyone of which forms a Green's function. It should be mentioned that in the framework of the shear lag model, the crack problem was represented in the same manner, see Landis and McMeeking (1999) for example. The problem in which a unit displacement jump is applied in the infinite layered composite domain is solved by the combined use of the representative cell method and the higher-order theory. In the representative cell method (Nuller and Ryvkin, 1980; Ryvkin and Nuller, 1997), the infinite periodic domain is reduced to a finite domain (representative cell) by the application of the discrete Fourier transform. The resulting boundary value problem for this representative cell is characterized by specific boundary conditions, referred to as the Born–von Karman type, that relate the opposite sides of the cell. This representative cell problem (in the transformed space) is solved by the higher-order theory according to which the displacements, which are governed by the continuum equations, are expanded into second order in terms of local coordinates (Aboudi et al., 1999). This combined approach was successfully employed for the solution of the fiber loss problem in periodically fiber reinforced composites (Ryvkin and Aboudi, 2007). In the latter paper several references to the representative cell method and higher-order theory can be found.

The paper is organized as follows. In Section 2, we start with the solution of the crack problem in a homogeneous material using the representative cell method and higher-order theory. This is followed by an illustration of the accuracy of the present approach by a comparison with the exact analytical solution. The solution of the cracked composite problem is presented in Section 3. Here, extensive parametric study (different crack tip locations, fiber volume fractions, elastic moduli ratios and Poisson's ratios) of the stress field caused by the applied tensile far-field loading is presented. In particular, the stress field ahead of the crack in the fiber and matrix regions and the normal and shear stresses in the broken and neighboring fibers are presented. Furthermore, the validity of the shear lag approximation is examined by a comparison with the average stresses computed from the obtained accurate stress distribution. The paper is concluded by several possible extensions of the proposed approach.

2. Solution of a crack in a homogeneous plane using the representative cell method and higher-order theory

In order to illustrate our approach for the analysis of a fiber reinforced material with a transverse crack, let us consider first the problem of a crack embedded in an infinite elastic plane that is subjected to a tensile loading. This problem of a Mode I Griffith crack is solved by combining the analyses of the representative cell method and higher-order theory. The solution is achieved by constructing a set of Green's functions as described in the following.

2.1. Modeling of a crack in an infinite plane using unit jump Green's functions

Consider a homogeneous elastic isotropic plane that is subjected to a remote tensile loading normal to a traction-free crack under plane strain conditions, see Fig. 1(a) where identical material properties should be

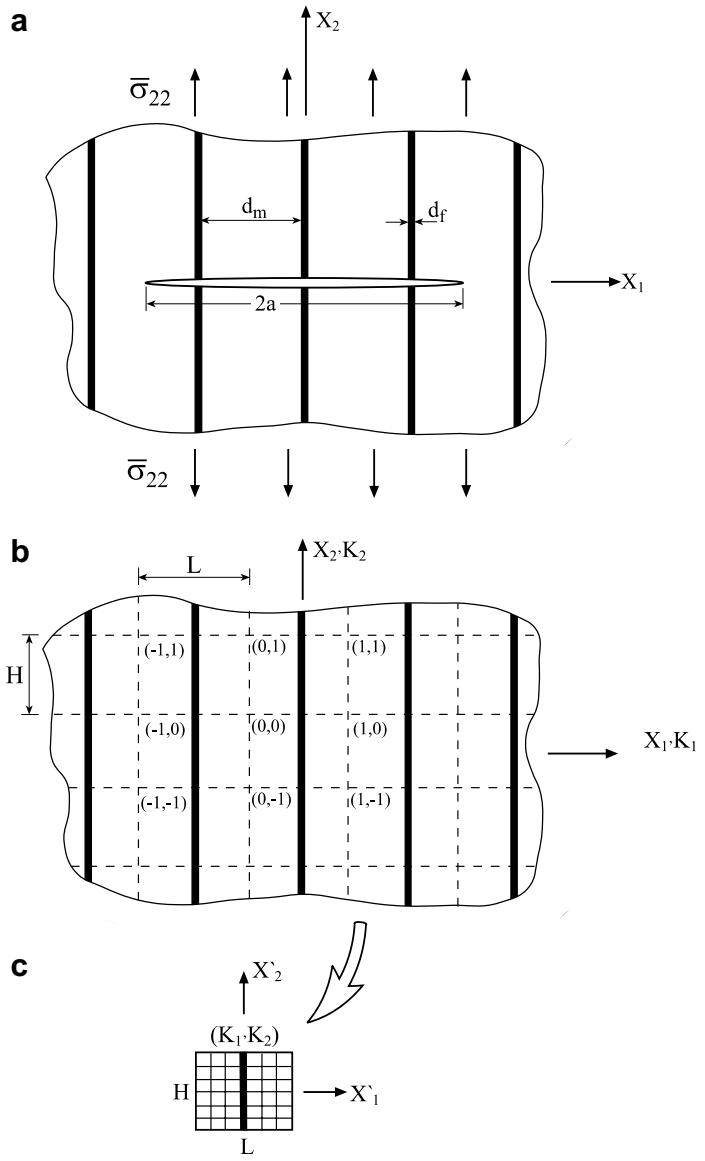

Fig. 1. (a) A periodically layered composite with am embedded crack normal to the layering subjected to a tensile stress $\bar{\sigma}_{22}$ at infinity [referred to the global coordinates (x_1, x_2)]. (b) The infinite plane is divided by repeating cells, labeled by (K_1, K_2) the size of every one of which is $L \times H$. (c) A characteristic cell (K_1, K_2) in which local coordinates (x'_1, x'_2) are introduced.

attributed to both fiber and matrix constituents. The crack region $-a \leqslant x_1 \leqslant a$ is divided into N segments whose length is $\Delta = 2a/N$, on everyone of which a unit displacement jump is applied. The location of the middle point of each segment is denoted by x_1^i, $i = 1, \ldots, N$. As a result, N elastic field distributions are generated. Let $G(x_1^i, x_1^j)$ denote the normal stress σ_{22} at $x_1 = x_1^i$ and $x_2 = 0$ caused by the application of the unit displacement jump at segment j. In order to model a traction-free surface of a crack in the region $-a \leqslant x_1 \leqslant a$ these Green functions are superposed in the following form:

$$\sum_{i=1}^{N} c_i G(x_1^i, x_1^j) = -\bar{\sigma}_{22}, \quad j = 1, \ldots, N \tag{1}$$

This forms a linear system of N algebraic equations for the determination of the coefficients c_i, $i = 1, \ldots, N$. It should be noted that for the present Mode I problem, symmetry guarantees the vanishing of the shear traction along the crack's line. Once these coefficients have been determined, the elastic field $U(x_1, x_2)$ at any point of the cracked plane can be determined as follows:

$$U(x_1, x_2) = \sum_{i=1}^{N} c_i U_i(x_1, x_2) + U_0(x_1, x_2) \tag{2}$$

where $U_i(x_1, x_2)$ is the elastic field that generated at point (x_1, x_2) by the application of the displacement jump at segment i and $U_0(x_1, x_2)$ is the corresponding elastic field at this point generated by the applied loading at infinity. It should by mentioned that in the framework of the shear lag theory, similar approach to the crack modeling by the construction of Green's functions was employed, see Sastry and Phoenix (1993) for example.

2.2. The determination of Green's functions

The determination of these Green's functions is obtained by the combined use of the representative cell method and higher-order theory. In accordance with the representative cell method the homogeneous plane is viewed as an assemblage of bonded identical cells labeled by the two indices (K_1, K_2) where $K_1, K_2 = 0, \pm 1, \pm 2, \ldots$, see Fig. 1(b) in which, as mentioned above, the existence of the fibers should be ignored. The infinite plane is described with respect to global coordinates (x_1, x_2). In addition, in each cell local coordinates (x_1', x_2') are introduced whose origin is located in its center, see Fig. 1(c). The elastic field generated by a unit displacement jump in cell $(0,0)$ is sought. It is applied along the segment $-\Delta/2 \leqslant x_1' \leqslant \Delta/2$ at $x_2' = 0$. The formulation of this plane problem is presented as follows.

In the absence of body forces, the equilibrium equations in any cell (K_1, K_2) are given by

$$[\sigma_{jk,k}]^{(K_1,K_2)} = 0, \quad j,k = 1,2; \quad K_1, K_2 = 0, \pm 1, \pm 2, \ldots \tag{3}$$

where $\sigma_{jk}^{(K_1,K_2)}$ are the stress components. For an elastic material they are given by

$$[\sigma_{jk}]^{(K_1,K_2)} = C_{jklm}[\epsilon_{lm}]^{(K_1,K_2)} \tag{4}$$

where C_{jklm} the elements of the stiffness tensor of the material and $\epsilon_{jk}^{(K_1,K_2)}$ are the strain tensor components. The strains are related to the displacement gradients in the standard form

$$[\epsilon_{jk}]^{(K_1,K_2)} = \frac{1}{2}\left[\frac{\partial u_j}{\partial x_k} + \frac{\partial u_k}{\partial x_j}\right]^{(K_1,K_2)} \tag{5}$$

In addition, continuity of displacements and tractions between adjacent cells should be imposed. Thus,

$$\left[u_j\left(x_1' = \frac{L}{2}, x_2'\right)\right]^{(K_1,K_2)} - \left[u_j\left(x_1' = -\frac{L}{2}, x_2'\right)\right]^{(K_1+1,K_2)} = 0, \quad -\frac{H}{2} \leqslant x_2' \leqslant \frac{H}{2} \tag{6}$$

$$\left[u_j\left(x_1', x_2' = \frac{H}{2}\right)\right]^{(K_1,K_2)} - \left[u_j\left(x_1', x_2' = -\frac{H}{2}\right)\right]^{(K_1,K_2+1)} = 0, \quad -\frac{L}{2} \leqslant x_1' \leqslant \frac{L}{2} \tag{7}$$

and

$$\left[\sigma_{1j}\left(x_1'=\frac{L}{2},x_2'\right)\right]^{(K_1,K_2)}-\left[\sigma_{1j}\left(x_1'=-\frac{L}{2},x_2'\right)\right]^{(K_1+1,K_2)}=0,\quad -\frac{H}{2}\leqslant x_2'\leqslant\frac{H}{2} \tag{8}$$

$$\left[\sigma_{2j}\left(x_1',x_2'=\frac{H}{2}\right)\right]^{(K_1,K_2)}-\left[\sigma_{2j}\left(x_1',x_2'=-\frac{H}{2}\right)\right]^{(K_1,K_2+1)}=0,\quad -\frac{L}{2}\leqslant x_1'\leqslant\frac{L}{2} \tag{9}$$

where $j=1,2,3$. This formulation is given for a generalized plane deformation case, but for the present case of a plane strain problem $j=1,2$.

The applied unit displacement jump in the x_2'-direction at the segment $-\Delta/2\leqslant x_1'\leqslant\Delta/2$ at $x_2'=0$ can be represented by the relations

$$\left[u_1(x_1',x_2'^{+})-u_1(x_1',x_2'^{-})\right]^{(K_1,K_2)}=0,\quad -\frac{\Delta}{2}\leqslant x_1'\leqslant\frac{\Delta}{2} \tag{10}$$

$$\left[u_2(x_1',x_2'^{+})-u_2(x_1',x_2'^{-})\right]^{(K_1,K_2)}=\delta_{K_1,0}\delta_{K_2,0},\quad -\frac{\Delta}{2}\leqslant x_1'\leqslant\frac{\Delta}{2} \tag{11}$$

where $\delta_{j,k}$ is the Kronecker delta.

The formulated problem, Eqs. (3)–(11), for infinite plane is reduced to a single representative cell problem by the application of the double discrete Fourier transform. This provides the transformed jth component of the displacement, for example, in the form:

$$\hat{u}_j(x_1',x_2',\phi_1,\phi_2)=\sum_{K_1=-\infty}^{\infty}\sum_{K_2=-\infty}^{\infty}u_j^{(K_1,K_2)}(x_1',x_2')\exp[\mathrm{i}(K_1\phi_1+K_2\phi_2)] \tag{12}$$

As a result, we obtain a representative cell problem for the transforms of the field variables in the finite region $-L/2\leqslant x_1'\leqslant L/2$, $-H/2\leqslant x_2'\leqslant H/2$. The governing equations in this region that correspond to Eqs. (3)–(11) are

$$\hat{\sigma}_{jk,k}=0,\quad j,k=1,2 \tag{13}$$

$$\hat{\sigma}_{jk}=C_{jklm}\hat{\epsilon}_{lm} \tag{14}$$

$$\hat{\epsilon}_{jk}=\frac{1}{2}\left[\frac{\partial\hat{u}_j}{\partial x_k}+\frac{\partial\hat{u}_k}{\partial x_j}\right] \tag{15}$$

$$\hat{u}_j\left(x_1'=\frac{L}{2},x_2',\phi_1,\phi_2\right)-\exp(-\mathrm{i}\phi_1)\hat{u}_j\left(x_1'=-\frac{L}{2},x_2',\phi_1,\phi_2\right)=0,\quad -\frac{H}{2}\leqslant x_2'\leqslant\frac{H}{2} \tag{16}$$

$$\hat{u}_j\left(x_1',x_2'=\frac{H}{2},\phi_1,\phi_2\right)-\exp(-\mathrm{i}\phi_2)\hat{u}_j\left(x_1',x_2'=-\frac{H}{2},\phi_1,\phi_2\right)=0,\quad -\frac{L}{2}\leqslant x_1'\leqslant\frac{L}{2} \tag{17}$$

and

$$\hat{\sigma}_{1j}\left(x_1'=\frac{L}{2},x_2',\phi_1,\phi_2\right)-\exp(-\mathrm{i}\phi_1)\hat{\sigma}_{1j}\left(x_1'=-\frac{L}{2},x_2',\phi_1,\phi_2\right)=0,\quad -\frac{H}{2}\leqslant x_2'\leqslant\frac{H}{2} \tag{18}$$

$$\hat{\sigma}_{2j}\left(x_1',x_2'=\frac{H}{2},\phi_1,\phi_2\right)-\exp(-\mathrm{i}\phi_2)\hat{\sigma}_{2j}\left(x_1',x_2'=-\frac{H}{2},\phi_1,\phi_2\right)=0,\quad -\frac{L}{2}\leqslant x_1'\leqslant\frac{L}{2} \tag{19}$$

$$\hat{u}_1(x_1',x_2'^{+},\phi_1,\phi_2)-\hat{u}_1(x_1',x_2'^{-},\phi_1,\phi_2)=0,\quad -\frac{\Delta}{2}\leqslant x_1'\leqslant\frac{\Delta}{2} \tag{20}$$

$$\hat{u}_2(x_1',x_2'^{+},\phi_1,\phi_2)-\hat{u}_2(x_1',x_2'^{-},\phi_1,\phi_2)=1,\quad -\frac{\Delta}{2}\leqslant x_1'\leqslant\frac{\Delta}{2} \tag{21}$$

where all field variables in the transform domain (hat-quantities) form complex quantities. Eqs. (16)–(19) refer to as the Born–von Karman type boundary conditions. It is readily seen that one needs to solve Eqs. (13)–(21) for the representative cell where the identity of the cell (K_1,K_2) disappeared.

The solution of this problem in the transform domain is carried by employing the higher-order theory that was described by Aboudi et al. (1999) and was successfully employed by Ryvkin and Aboudi (2007) for the

solution of fiber loss problem. In the framework of this theory, the representative cell domain $-L/2 \leqslant x_1' \leqslant L/2$, $-H/2 \leqslant x_2' \leqslant H/2$ is divided into rectangular subcells, Fig. 1(c), in everyone of which the transformed displacements are represented by a second-order polynomial. The transformed equilibrium equation and displacements and tractions continuity conditions between the subcells are imposed in the average (integral) sense.

Once this solution has been achieved, the actual elastic field can be readily determined at every point of any desired cell (K_1, K_2) of the infinite plane by the inverse transform formula

$$u_j^{(K_1,K_2)}(x_1', x_2') = \frac{1}{4\pi^2}\int_{-\pi}^{\pi}\int_{-\pi}^{\pi}\hat{u}_j(x_1', x_2', \phi_1, \phi_2)\exp[-\mathrm{i}(K_1\phi_1 + K_2\phi_2)]\mathrm{d}\phi_1\,\mathrm{d}\phi_2 \tag{22}$$

In practice, the solution of Eqs. (13)–(21) is determined for a spectrum of $-\pi \leqslant \phi_1 \leqslant \pi$, $-\pi \leqslant \phi_2 \leqslant \pi$ and the double integrals in (22) are approximated by the Gauss numerical integration (say), yielding

$$u_j^{(K_1,K_2)}(x_1', x_2') \approx \frac{1}{4\pi^2}\sum_{m_1=-M_1}^{M1}\sum_{m_2=-M_2}^{M2} w_{m_1,m_2}\hat{u}_j(x_1', x_2', (\phi_1)_{m_1}, (\phi_2)_{m_2}) \times \exp[-\mathrm{i}(K_1(\phi_1)_{m_1} + K_2(\phi_2)_{m_2})] \tag{23}$$

where $(\phi_1)_{m_1}$, $(\phi_2)_{m_2}$ are the Gauss roots and w_{m_1,m_2} are the corresponding weighting factors.

In Fig. 2, a comparison between the present approach and the exact analytical solution (see Sneddon, 1951, for example) for a crack embedded in an infinite homogeneous elastic plane that is subjected to a remote tensile loading $\bar{\sigma}_{22}$ is presented. Both the stress $\sigma_{22}(x_1, x_2 = 0)$ and the opening displacement $u_2(x_1, x_2 = 0)$ (which has been normalized with respect to the shear modulus μ of the material) at the crack plane are shown. It is readily observed that excellent agreements between the two solutions exists. The present solution was achieved by a discretizing the representative cell into 50×4 subcells and by employing 64 Gauss points of integration. The 50 subcells divide the interval $-L/2 \leqslant x_1' \leqslant L/2$ along the crack, whereas the 4 subcells divide the interval $-H/2 \leqslant x_2' \leqslant H/2$. It should be noted that square subcells have been employed so that $H/L = 0.08$. The present approach for the solution of the problem for an infinite domain requires for each pair (ϕ_1, ϕ_2) the solution of a system of $50 \times 4 \times 24$ linear algebraic sparse equations which is obtained from the higher-order theory.

As was mentioned above, the crack line is divided into several short intervals which corresponds to the sides of the subcells of the higher-order theory. The actual crack is generated by a superposition of the small cracks defined over these intervals. Since the higher-order theory analysis is based on averaged field quantities, the obtained excellent agreement with the analytical solution shown in Fig. 2 can be expected. This fact can be explained by the results reported by Kachanov (1985, 1987) who considered the problem of several interacting

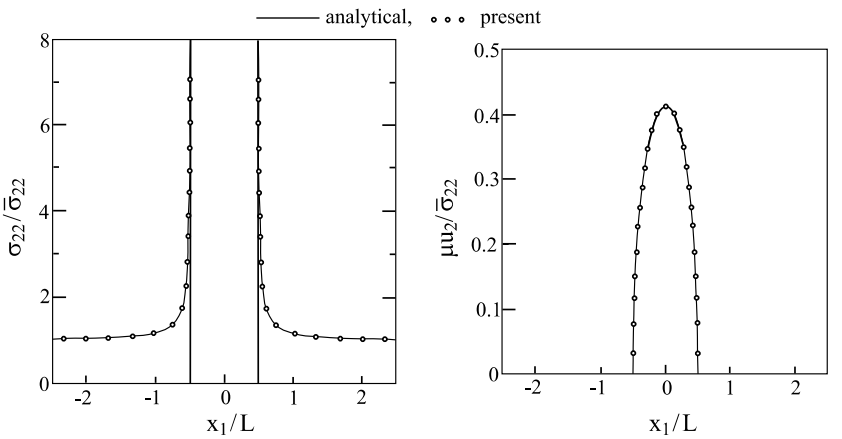

Fig. 2. A crack of length $2a/L = 1$ in a homogeneous plane subjected to a tensile normal stress loading $\bar{\sigma}_{22}$ at infinity. Comparisons between the normal stress σ_{22} and displacement u_2 along the plane of the crack $x_2 = 0$ as predicted by the present approach and the exact analytical solution.

cracks embedded in a homogeneous plane. He found that an analysis based on averaged stresses provides accurate results.

3. Crack in a fiber reinforced composite

The analysis of fiber reinforced composites with a transverse crack as shown in Fig. 1(a), in which the widths of the fiber and matrix are denoted by d_f and d_m, respectively, is carried out in the same manner as for a crack in an infinite homogeneous plane. The fiber and matrix constituents are assumed to be isotropic with Young's moduli and Poisson's ratios given by: E_f, E_m, ν_f and ν_m. This problem represents a two-dimensional model of a unidirectional fiber reinforced composite with broken fibers. In the case of a homogeneous plane, both dimensions of the representative cell (L and H) defined by the translational symmetry of the plane were arbitrary. In the present case, however, the translational symmetry in the x_1-direction is determined by the periodic fiber arrangement. It is convenient to locate the vertical boundaries of the cells (K_1, K_2) at the middle line between the fibers as shown in Fig. 1(b). In addition, since each cell (K_1, K_2) will include two types of materials (fiber and matrix) the stiffness matrix C_{jklm} which is independent on (K_1, K_2) is not uniform within the cells. Accordingly, the representative cell in the transform domain is divided into subcells. The fibers are incorporated by a suitable filling of the subcells by the their material properties. It should be noted that in the case of a crack in a homogeneous plane all Green's functions calculated from applied displacement jumps at different segments are identical except for a shift in the x_1-direction. In the presence of the fibers this property does not exist. Consequently, one has to calculate all these Green's functions that correspond to displacement jumps applied over all segments. Furthermore, in the present case of fiber reinforced composites, the average far-field stress $\bar{\sigma}_{22}$ is redistributed in the fiber and matrix constituents. The exact expressions for the fiber and matrix far-field stresses can be determined in terms of the material and geometrical properties of the fiber and matrix phases. These expressions can be well approximated in conjunction with the mixture's law by

$$\sigma_{22}^{f(\infty)} = \frac{E_f}{E^*}\bar{\sigma}_{22}, \qquad \sigma_{22}^{m(\infty)} = \frac{E_m}{E^*}\bar{\sigma}_{22} \tag{24}$$

where $E_2^* = (d_f E_f + d_m E_m)/(d_f + d_m)$ being the effective Young's modulus of the (uncracked) doubly periodic layered composite in the x_2-direction. Consequently, Eq. (1) takes the form

$$\sum_{i=1}^{N} c_i G(x_1^i, x_1^j) = \begin{cases} -\sigma_{22}^{f(\infty)} & \text{in the fiber region} \\ -\sigma_{22}^{m(\infty)} & \text{in the matrix region} \end{cases} \tag{25}$$

with $j = 1, \ldots, N$.

Several distinct situations must be addressed. Consider first the case in which the crack is located within the cell $(K_1 = 0, K_2 = 0)$ (i.e., $2a < L$). Here the number of Green's functions N_G is equal to the number of segments, namely $N_G = N = 2a/\Delta$. In the extreme case of a crack extending over the entire cell (i.e., $2a = L$), $N_G = N = L/\Delta$. On the other hand, when the crack extends beyond this cell (i.e., $2a > L$) the number of Green's functions is still equal to $N_G = L/\Delta$ and $N = 2a/\Delta$. This is because due to the translational symmetry of the composite the following equality holds

$$G(x_1^i, x_1^j) = G(x_1^i + nL, x_1^j + nL) \tag{26}$$

where $n = 0, \pm 1, \pm 2, \ldots$ Thus any value of Green's function outside the repeating unit cell can be expressed in terms of its values within the cell $(K_1 = 0, K_2 = 0)$.

It should be emphasized that the present investigation, based on a continuum approach, enables the determination of the elastic field anywhere in the fiber and matrix regions without the utilization of any simplifying assumption.

Fig. 3 exhibits the normal stress σ_{22} along the crack line $x_2 = 0$ for three different cases in all of which the fiber volume fraction $v_f = d_f/L = 0.48$ and the ratio between the fiber and matrix Young's moduli is $E_f/E_m = 10$. The stresses are induced by the application of a remote average normal stress $\bar{\sigma}_{22}$. The Poisson's ratios of the fiber and matrix, here and in all following cases unless otherwise mentioned, are $\nu_f = \nu_m = 0.2$. In Fig. 3(a), the normal stress is shown for a cracked fiber (intact matrix) in cell $(K_1 = 0, K_2 = 0)$ in which

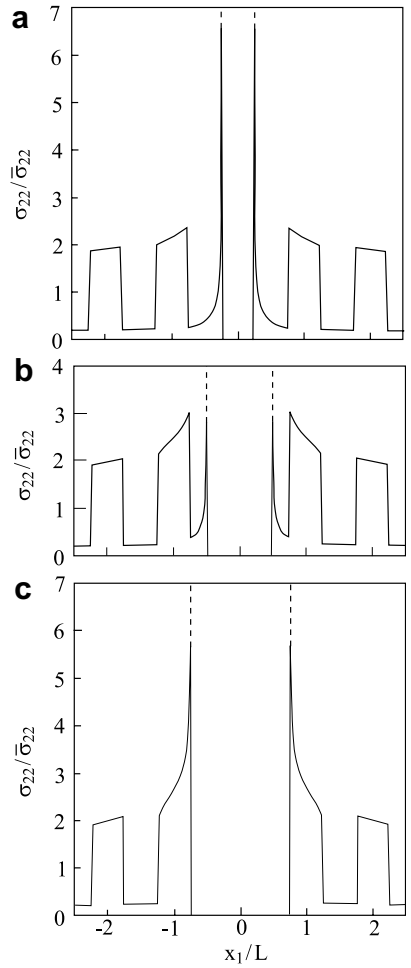

Fig. 3. The normal stress variation along the crack line $x_2 = 0$ of the cracked fiber reinforced material subjected to a remote stress $\bar{\sigma}_{22}$ at infinity. (a) Cracked fiber (intact matrix), (b) half matrix broken, (c) matrix broken.

the length of the crack is $2a = d_f$. Fig. 3(b) and (c) show the cases of half matrix broken ($2a = L$) and broken matrix ($2a = 2L - d_f$), respectively. In all cases the singularity at the tip of the crack is well observed. In order to explain the differences in the stress amplitudes near the crack tips in these three different cases, let us recall that in the absence of a crack, the normal stress in the fiber is higher than the one induced in the matrix. In the case Fig. 3(a), the crack is located within the fiber (strong material) and its tip is approaching the matrix (soft material). In this case the stress singularity is known (Cook and Erdogan, 1972) to be stronger than that of a crack terminated within a homogeneous material. This is in agreement with the results depicted in Fig. 3(a) and (b). In Fig. 3(c) the crack is within the matrix and its tip is approaching the fiber. Here the stress singularity is known to be weaker than that in the homogeneous case. However, the contribution of the high remote stress jump in the fiber results in a relatively high stress amplitude at the vicinity of the crack's tip. Thus, as shown in Fig. 3(c), the stress at the crack's tip in the fiber, is higher than that in Fig. 3(b).

An examination of Fig. 3 reveals that the stress distribution within the fiber is not uniform. This is especially so for the fibers in vicinity of the crack. The maximum stress in the fiber is obtained at the fiber–matrix interface that is closer to the crack tip. For the case of a composite with fiber volume fraction of $v_f = 0.48$ and $E_f/E_m = 10$ with a half broken matrix shown in Fig. 3(b) for example, the ratio of the maximum stress $\sigma_{22}^{f(max)}$ to the average stress $\langle \sigma_{22}^{f} \rangle$ is 1.18. Hence the estimation of the composite's strength based on the average stress in the first unbroken fiber as it is done in the shear lag theory may significantly overestimate this

property. It should be mentioned however that for lower values of fiber volume fractions the estimation of the composite's strength based on the average normal stress in the fiber is more reliable. Fig. 3 also shows the expected result that the effect of the crack rapidly diminishes with the distance away from its tip along its plane. This observation is in agreement with the results obtained by the shear lag theory (Hikiami and Chou, 1990).

The shear lag theory can predict the average normal stress in the fiber $\langle\sigma_{22}^{f}\rangle$ only. Therefore, it should interesting to compare the shear lag prediction of $\langle\sigma_{22}^{f}\rangle$ with the present continuum approach. To this end, the dependence of the normalized average stress in the fiber (referred to as stress concentration factor) is shown in Fig. 4(a) against the matrix and fiber elastic moduli ratio E_m/E_f for a fiber volume fraction of $v_f = 0.48$. The solid lines correspond to the present theory prediction in the cases of intact matrix, half broken matrix and broken matrix. In the limiting case of a homogeneous material ($E_m/E_f = 1$) the stress concentration factor is given by the closed-form expression

$$\frac{\langle\sigma_{22}^{f}\rangle}{\sigma_{22}^{f(\infty)}} = \int_{a+b}^{a+b+d_f} \frac{x\,dx}{\sqrt{x^2+a^2}} = \sqrt{\left(\frac{a+b}{d_f}+1\right)^2 - \left(\frac{a}{d_f}\right)^2} - \sqrt{\left(\frac{a+b}{d_f}\right)^2 - \left(\frac{a}{d_f}\right)^2} \tag{27}$$

where b is the distance from the crack tip to the first unbroken fiber. For intact matrix, half broken matrix and broken matrix b is equal to d_m, $d_m/2$ and 0, respectively. These limiting cases are indicated in Fig. 4(a) by empty circles. Excellent agreements with Eq. (27) are obtained in the case of intact and half broken matrix. In the case of a broken matrix the present analysis yields a somewhat lower value in this limiting case. This can be attributed to the fact that the integration region in Eq. (27) includes a singularity which cannot be captured by the discretization.

Fig. 4(a) shows also the other limiting case of $E_m/E_f \to 0$. Here the classical shear lag theory of Hedgepeth (1961) predicts the value of 4/3 which is in good agreement with our results for broken and half broken matrix. Beyerlein and Landis (1999), who improved the classical shear lag model by accounting for the ability of the matrix to carry tensile stresses, characterized the elastic properties and geometry of the fiber–matrix composite by the single parameter: $\rho = E_m d_m/E_f d_f$. In the present analysis however, the complete set of parameters: E_f, E_m, v_f, v_m, d_f, d_m are independently required. In Fig. 4(a), several data points provided by Beyerlein and Landis (1999) for the case of intact and broken matrix are included. It should be mentioned that the present results and Beyerlein and Landis (1999) data are in close agreement for the case of intact matrix. For the broken matrix, on the other hand, the two approaches are in good agreement only for a relatively stiff fibers.

As was previously mentioned, the use of the average normal stress in the fiber may overestimate the composite's predicted strength. Therefore, results shown in the following present the maximum normal stress in the fiber. Fig. 4(b) presents the maximum normal stress in the unbroken fiber of a half broken matrix at

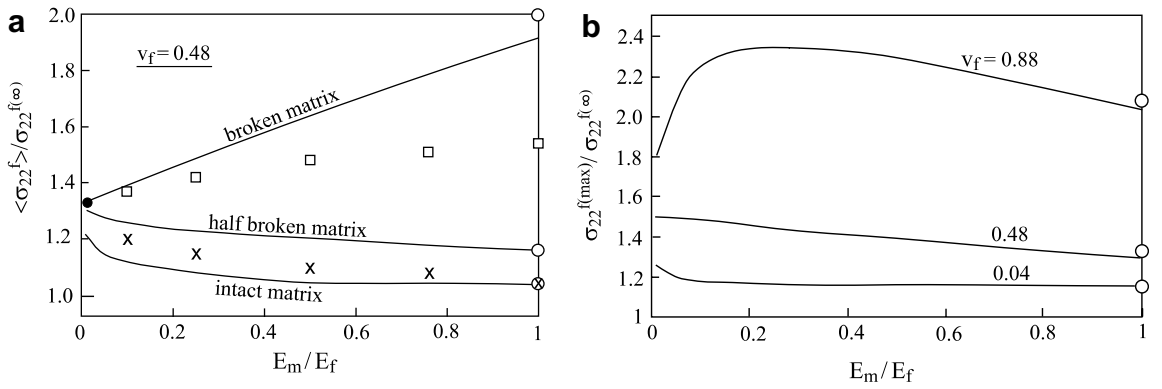

Fig. 4. (a) The variation of the normalized average normal stress in the unbroken fiber against the ratio E_m/E_f for the cases of intact matrix, half matrix broken and broken matrix. The symbols ●, □, × and ○ show the classical shear lag theory prediction, the prediction of Beyerlein and Landis (1999) for broken and intact matrix, and the limiting analytical prediction of Eq. (27), respectively. (b) The variation of the normalized maximum normal stress in the first unbroken fiber against the ratio E_m/E_f for three values of fiber volume ratios in the case of a half broken matrix. The symbols ○ denote the limiting cases given by Eq. (28).

the crack plane against the ratio E_m/E_f, for fiber volume fraction $v_f = 0.04$,0.48 and 0.88. Also shown in this figure are the limiting homogeneous case, $E_f = E_m$, for which

$$\frac{\sigma^{f(max)}}{\sigma_{22}^{f(\infty)}} = \frac{2a + d_m}{\sqrt{4ad_m + d_m^2}} \tag{28}$$

The figure shows that good agreement with the values obtained by this equation exists. As the fiber volume fraction increases, the distance between the crack tip and points at which the stress is evaluated decreases. As a result, and as it is seen in the figure, the small deviation from the analytical results increases as the volume fraction increases. This also implies that for a given ratio E_m/E_f, the maximum stress increases as the volume fraction increases. As it can be observed from the figure, for small and moderate values of v_f, the influence of the moduli ratio is weak. For the higher value of v_f a different behavior can be observed. The maximum stress decrease with the fiber stiffness increase for small ratios E_m/E_f can be attributed to the fact that under such circumstances the deformation becomes less localized. Thus, large amount of matrix material involves in the deformation and prevents the broken fiber displacement and crack opening.

The propagation of a transverse crack in a fiber reinforced material can be viewed as discrete process where at each stage the crack advances through the fiber and certain part of the surrounding matrix. The amount of the matrix which fails at each fracture event is unknown. This amount determines the correct location of the crack tip in the static analysis of the crack in fiber reinforced composite. In the framework of the classical shear lag theory, there are two possibilities for the assignment of the crack tip which are either at the end of the fiber region (i.e., an intact matrix case) or at the end of matrix region (i.e., broken matrix case). It should be noted that the difference between these two cases decreases with the increasing of the fiber–matrix elastic moduli ratio. To this end, it is worthwhile to note (Cook and Erdogan, 1972), that the power of the stress singularity in front of a crack embedded into a stiff material and terminating at the interface with a weak one is stronger than $-1/2$ and weaker than this quantity when the order of the materials is reversed. As a result, the stress intensity factor in the first case of a crack approaching the interface will tend to infinity, and to zero in the second case. Consequently, a crack approaching the interface with a weak/stiff material will be unstable/stable. The exact condition for the crack stability/instability was established by Nuller et al. (2006). Based on this discussion, the actual crack tip has to be located somewhere within the matrix region. In the improved shear lag analysis, Beyerlin et al. (1996) chose the location of the crack tip within the matrix domain to be at distance $L/3$ from the center line of the first unbroken fiber. In the following results the value of $L/2$ was adopted, thus forming a fiber reinforced composite with a half matrix broken.

It is well known that for a sufficiently long crack embedded in a homogeneous material the stress state in the vicinity of the crack tip becomes self similar and proportional to the square root of the crack length. Indeed, the normal stress σ_{22} at distance b from the crack tip is given by

$$\frac{\sigma_{22}}{\sigma_{22}^{(\infty)}} = \frac{a + b}{\sqrt{2ab + b^2}} \approx \sqrt{\frac{a}{2b}} \tag{29}$$

It is important to establish such a property in the present case of a cracked fiber reinforced composite. To this end, let us consider cracks of different lengths in which their tips are located in the middle distance between two adjacent fibers thus forming the half matrix broken case. In Fig. 5, the normalized maximum stress in the first intact fiber divided by the square root of the crack length are shown against the number of broken fibers (which is equal to the normalized crack length: $2a/L$) for $E_f/E_m = 20$ and 100 and $v_f = 0.04$. It is readily observed that asymptotic values are rapidly achieved at about 10 broken fibers. For a reference, the homogeneous case, which is given by the exact expression in Eq. (29) with $b = d_m/2$, is also shown by a solid line exhibiting a similar behavior. The behavior shown in this figure for cracked fiber composites is in complete agreement with the analytical results obtained from the shear lag theory (Dharani et al., 1983; Beyerlin et al., 1996). It is also in agreement with the data obtained by the improved shear lag model of Beyerlein and Landis (1999). It is worth mentioning that a similar saturation behavior was observed in a square honeycomb cellar material (Huang and Gibson, 1991) which also forms a type of periodic composites.

Let us investigate next the behavior of the axial stress σ_{22}^f in the fibers induced by the crack. Fig. 6(a) shows the normalized axial stress due to a single broken fiber with a crack length $2a = L$ (i.e., a half matrix broken).

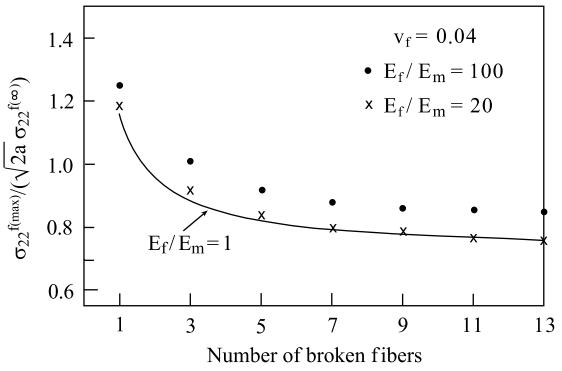

Fig. 5. The normalized maximum normal stress divided by the square root of the crack length against the number of broken fibers for composites with half matrix broken and $v_f = 0.12$. The solid shows the corresponding case of a cracked homogeneous plane $E_f/E_m = 1$.

The figure shows the induced stress along the broken fiber at $x_1 = d_f/2$ and the maximum stresses in the next two intact ones (i.e., at $x_1 = L - d_f/2$ and $x_1 = 2L - d_f/2$) in the case of $v_f = 0.12$ and $E_f/E_m = 10$. As was previously exhibited by Fig. 3, these maxima occur within the fiber at the fiber–matrix interfaces that are the nearest to the crack tip. It is readily observed that the effect of the single fiber breakage is localized within a region of about eight crack lengths. The stress in the broken fiber increases rapidly to its far-field value whereas in the neighboring intact fibers, the stress concentration effect can be readily observed in front of the crack at $x_2 = 0$. A significant reduction in the stress concentration from the first to the second intact fiber takes place. Fig. 6(a) exhibits the stress σ_{22}^f in the first intact fiber at the fiber–matrix interface where the maximum is obtained (i.e., at $x_1 = L - d_f/2$). It is interesting to show this stress at the second fiber–matrix interface of this intact fiber (i.e. $x_1 = L + d_f/2$). A comparison between the normal stresses at these two locations is shown in Fig. 6(b). It can be immediately observed that the latter case there is a peculiar rise and fall in the fiber stress profile. This is in agreement with the result of Beyerlein and Landis (1999) who obtained a similar behavior of the average axial stress in the fiber in conjunction with their improved shear lag analysis for some parameter combination of the composite.

The influence of Young's moduli ratio E_f/E_m on the normalized axial stress σ_{22}^f along the fiber is examined in Fig. 7 for $v_f = 0.12$. Fig. 7(a) exhibits this stress along the broken fiber. As expected, the stress in the broken fiber increases more slowly as its stiffness increases. The axial stress variation in the case of $E_f/E_m = 1$ coincides with the analytical solution for a crack embedded in a homogeneous plane. The axial stress variation in the

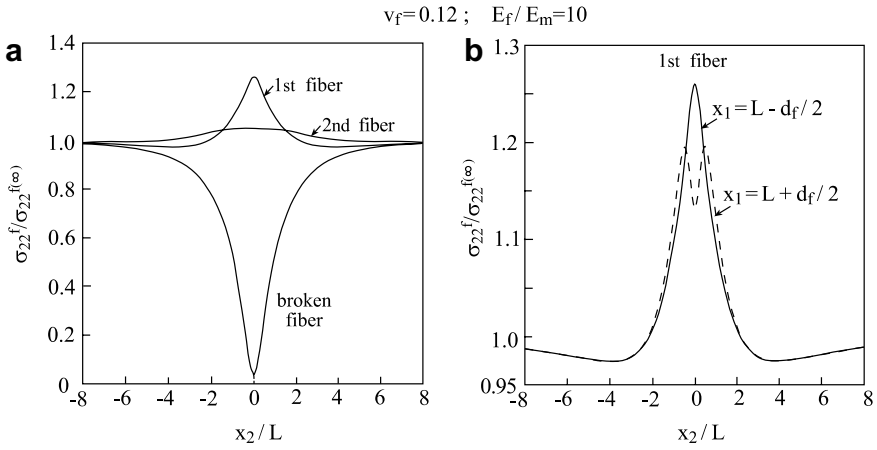

Fig. 6. (a) The axial fiber stress variation along the fiber–matrix interface of the broken fiber ($x_1 = d_f/2$), the first intact fiber ($x_1 = d_f/2 + d_m$) and second intact fiber ($x_1 = 3d_f/2 + 2d_m$), see inset of Fig. 8(a). (b) A comparison between the axial fiber stress variation along the fiber–matrix interface of the first intact fiber at $x_1 = L \pm d_f/2$.

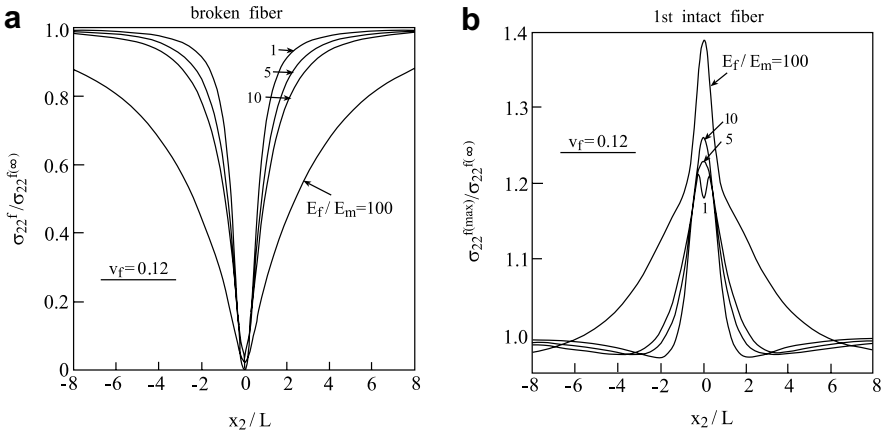

Fig. 7. The axial fiber stress variation along the fiber–matrix interface for several values of E_f/E_m. (a) Fiber stress variation within the broken fiber ($x_1 = d_f/2$), (b) fiber stress variation within the first intact fiber ($x_1 = d_f/2 + d_m$), see inset of Fig. 8(a).

first intact fiber, Fig. 7(b), is obtained at $x_1 = L - d_f/2$. Here, the maximum value of stress increases as Young's moduli ratio E_f/E_m increases and its decay becomes slower. This is due to the fact that a high modulus fiber carries a large portion of the far-field loading so that its breakage causes a more significant effect. It is interesting that the stress variation in the homogeneous case $E_f/E_m = 1$, which coincides with the analytical solution, exhibits the peculiar non-monotonic behavior that was mentioned before.

It is important to study the induced shear stress σ_{12} at the fiber–matrix interface due to the crack's existence, since it may provide information on the possibility of the debonding phenomenon. In Fig. 8, the normalized shear stresses at the fiber–matrix interface along the broken fiber and along the first intact fiber are shown for various values of Young's moduli ratio E_f/E_m and $v_f = 0.12$. Recall that a half broken matrix case is considered in which the crack length $2a = d_f + d_m$, see Fig. 1(a). In the broken fiber case, Fig. 8(a), the shear stresses at the interface exhibit a singular behavior caused by the contact of two different materials ($E_f/E_m \neq 1$) at the traction-free crack face: $x_2 = 0$. These singularities appear in very narrow regions in the form of steep variations which are not shown. In the homogeneous case ($E_f/E_m = 1$), the singularity disappears and $\sigma_{12} = 0$ at $x_2 = 0$. Here too, the resulting stresses as predicted by the present model coincide with the exact solution for a crack in a homogeneous plane. In all cases, the shear stresses at the interface of the first intact fiber, Fig. 8(b), start from zero at $x_2 = 0$ due to the symmetry of the problem. It is interesting to note that the shear

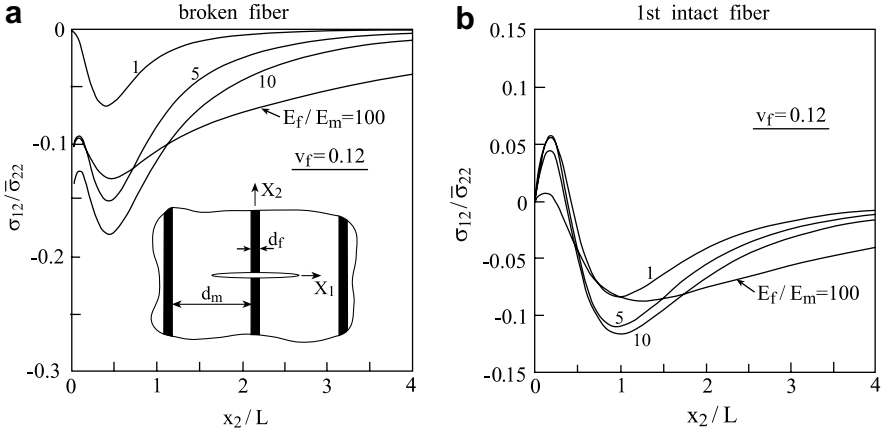

Fig. 8. The shear stress variation along the fiber–matrix interface for several values of E_f/E_m. (a) Shear stress variation at the interface of the broken fiber ($x_1 = d_f/2$). (b) Shear stress variation at the interface of the first intact fiber ($x_1 = d_f/2 + d_m$).

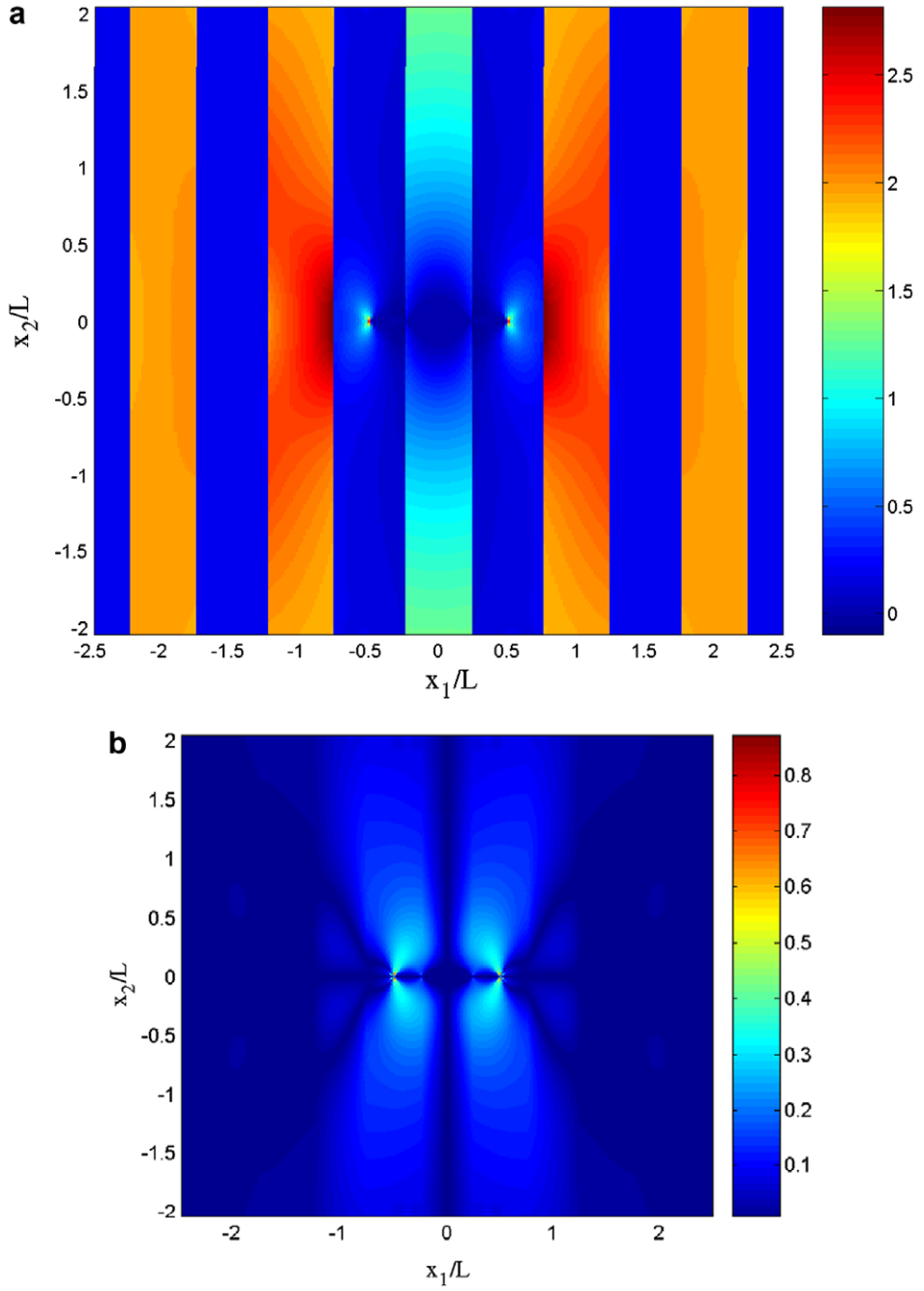

Fig. 9. Color plot of the stress distribution in the region $-2.5 \leqslant x_1/L \leqslant 2.5$, $-2 \leqslant x_2/L \leqslant 2$ for a composite with a half matrix broken characterized by $E_f/E_m = 10$ and $v_f = 0.48$. (a) Stress distribution of $\sigma_{22}/\bar{\sigma}_{22}$, (b) stress distribution of $|\sigma_{12}|/\bar{\sigma}_{22}$.

stresses in both cases of broken and intact fibers exhibit a non monotonic behavior. As in the axial stress case, the rate of the shear stress decay decreases as the Young's moduli ratio E_f/E_m increases. Fig. 8 shows that each curve has its own maximum value at the vicinity of the points $x_2/L = 0.5$ and $x_2/L = 1$ for the broken and intact fiber, respectively. It should be noted that the values of these maxima depend on E_f/E_m ratio in a non-monotonic manner. Consequently, an increase of E_f/E_m ratio may lead to an increase or decrease of the maximum shear stress (debonding stress) in the cracked composite.

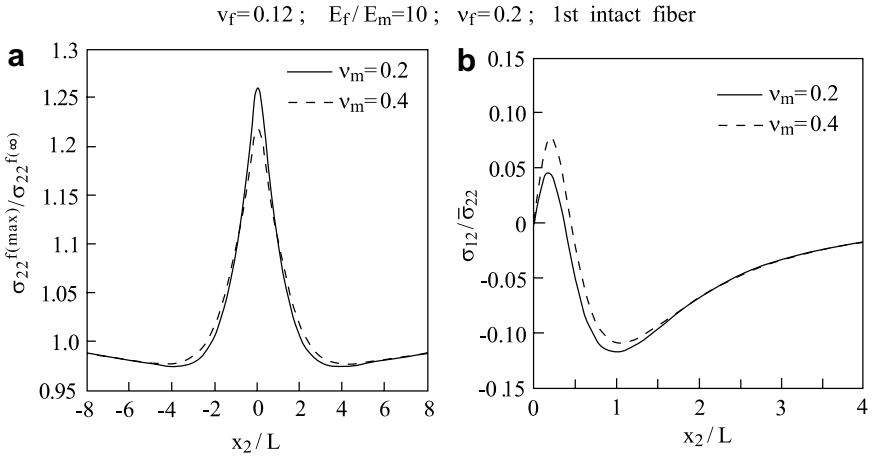

Fig. 10. (a) Comparison between the axial fiber stress variation along the fiber–matrix interface of the first intact fiber for different values of the Poisson's ratio of the matrix. (b) Comparison between the interfacial shear stress along the fiber–matrix interface of the first intact fiber for different values of the Poisson's ratio of the matrix.

It should be noted that the resulting stresses induced in the matrix region between the broken and intact fiber of the composite approach the ultimate value of the matrix stress σ_m^U for an externally applied loading which is much less than the failure stress of the fiber σ_f^U (for glass fibers and epoxy matrix, for example, $\sigma_f^U = 3.4$ GPa and $\sigma_m^U = 70$ MPa). The high stresses in the matrix will be blunted by some form of local yielding or debonding over several fiber diameters.

Color plots that present the normal stress σ_{22} and the absolute value of the shear stress $|\sigma_{12}|$ are shown in Fig. 9 in the region $-2.5 \leqslant x_1/L \leqslant 2.5$, $-2 \leqslant x_2/L \leqslant 2$ for a composite with a half matrix broken characterized by $v_f = 0.48$ and $E_f/E_m = 10$. It should emphasized that the present analysis provides the stress field in the infinite plane and Fig. 9 shows the stress field distribution in a region of interest. It is readily seen from Fig. 9 that the effect of the single fiber breakage is localized within a region extending over several values of $L = d_f + d_m$. Fig. 9(a) illustrates the non-uniform normal stress distribution across the fibers which indicates that the use of the average stress in the intact fibers in the present case of relatively high fiber volume fraction for estimating the strength of the composite might be questionable. Fig. 9(a) shows also the different types of behavior of stress along opposite sides of the first unbroken fiber that has been discussed in Fig. 6(b). The shear stress distribution shown in Fig. 9(b) indicates the singular stress behavior at the crack tips. In addition, another stress singularity can be observed at the intersection of the interface of the broken fiber and the crack's face as was discussed previously in connection to Fig. 8(a). Finally, a stress concentration along the boundaries of the broken matrix regions can be clearly observed. A color plot of the other normal stress σ_{11} parallel to the crack (not shown) reveals that the crack surfaces are subjected to a compressive stress that switches to small tensile stress ahead of the crack. These stresses do not indicate the possibility of fiber–matrix debonding without an interfacial shear component.

The present approach enables to examine the effect of the Poisson's ratio changes of the materials. In Fig. 10, the influence of the matrix Poisson's ratio is illustrated. This figure shows the axial stress in the first intact fiber and the interfacial shear stress at $x_1 = L - d_f/2$ for two values of the matrix Poisson's ratio: $v_m = 0.2$ and 0.4. It is shown that except for the values of the maxima of the stresses, no appreciable changes take place. This figure indicates that the increase of the matrix Poisson's ratio leads to a decrease of the maximum of the normal as well as the shear stress.

4. Conclusions

A continuum approach for the analysis of a periodically fiber reinforced material with a transverse crack, subjected to a far-field tensile loading has been presented. This was performed by combining two approaches, namely, the representative cell method and the higher-order theory. As a result, accurate elastic field can be

readily computed at any point in the infinite domain. This approach was found to be efficient and convenient for the computation of the elastic field everywhere in both fiber and matrix constituents. In the special case of a crack embedded in a homogeneous material, the elastic field provided by the present method is in excellent agreement with the analytical solution. The effects of several parameters that characterize the geometry and material properties of the cracked composite as well as the number of broken fibers and the locations of the crack tip on the resulting elastic field are studied.

The elastic field for several crack tip locations within the matrix region was examined and comparisons of the resulting average values of the axial stress with the shear lag predictions were performed. It turns out that the shear lag theory provides a reliable prediction of the average stress in the fiber in the case of an intact matrix. It was found however that the average of the actual stress distribution, upon which the shear lag theory is based, might not be, for some composite's parameters, a reliable indicator for the fiber failure. Indeed, it was found in a specific case that the maximum tensile stress in the first intact fiber is about 18% higher than the average stress.

The analysis of the cracked composite with different crack's lengths reveals that after about ten fiber breakages the elastic field in the vicinity of the tip becomes self-similar. This result was found to be insensitive to the ratio of the fiber to matrix Young's moduli. The effect of the Poisson's ratio of the matrix on the resulting stress distribution was examined and found to be insignificant.

The present methodology has been employed for a composite with a single transverse crack. It is possible however to consider a composite with several transverse cracks as well as cracks parallel to the fibers including debonding interfacial cracks. This is performed by establishing the corresponding Green's functions by the application of normal and shear displacement jumps from which the induced normal and shear stresses can be computed. Furthermore, the present analysis can be employed for the investigation of composites with mode II and mode III longitudinal and transverse cracks.

Due to the inherent continuum approach of the method, one can easily consider cracked periodic composites with anisotropic phases (e.g., transversely isotropic carbon fibers). Another important extension of the present approach is its application for the prediction of the behavior of composites with broken fiber in the framework of the three-dimensional theory of elasticity in which a triple discrete Fourier transform should be involved.

References

Aboudi, J., Pindera, M.-J., Arnold, S.M., 1999. Higher-order theory for functionally graded materials. Composites: part B (Engineering) 30, 777–832.

Beyerlein, I.J., Landis, C.M., 1999. Shear-lag model for failure simulations of unidirectional fiber composites including matrix stiffness. Mech. Mater. 31, 331–350.

Beyerlin, I.J., Phoenix, S.L., Sastry, A.M., 1996. Comparison of shear-lag theory and continuum fracture mechanics for modeling fiber and matrix stresses in an elastic cracked composite lamina. Int. J. Solids Struct. 33, 2543–2574.

Cook, T.S., Erdogan, F., 1972. Stress in bonded materials with a crack perpendicular to the surface. Int. J. Eng. Sci. 10, 677–697.

Dharani, L.R., Jones, W.F., Goree, J.G., 1983. Mathematical modeling of damage in unidirectional composites. Eng. Fract. Mech. 17, 555–573.

Hedgepeth, J.M., 1961. Stress concentrations in filamentary structures, NASA TN D-882.

Hedgepeth, J.M., Van Dyke, P., 1967. Local stress concentrations in imperfect filamentary composite materials. J. Compos. Mat. 1, 294–309.

Hikiami, F., Chou, T.W., 1990. Explicit crack problem solutions of unidirectional composites: elastic stress concentrations. AIAA J. 28, 499–505.

Huang, J.S., Gibson, L.J., 1991. Fracture toughness of brittle foams. Acta Metall. Mater. 39, 1627–1636.

Kachanov, M., 1985. A simple technique of stress analysis in elastic solids with many cracks. Int. J. Fracture 28, R11–R19.

Kachanov, M., 1987. Elastic solids with many cracks: a simple method of analysis. Int. J. Solids Struct. 23, 23–43.

Landis, C.M., McMeeking, R.M., 1999. Stress concentrations in composites with interface sliding, matrix stiffness and uneven fiber spacing using shear lag theory. Int. J. Solids Struct. 36, 4333–4361.

Nedele, M.R., Wisnom, M.R., 1994. Three-dimensional finite element analysis of the stress concentration at a single fibre break. Compos. Sci. Technol. 51, 517–524.

Nuller, B., Ryvkin, M., 1980. On boundary value problems for elastic domains of a periodic structure deformed by arbitrary loads. Proc. State Hydraulic Inst. 136, 49–55, Energia, Leningrad (in Russian).

Nuller, B., Ryvkin, M., Chudnovsky, A., 2006. A closed-form solution for a crack approaching an interface. J. Mech. Mater. Struct. 1, 1405–1423.

Ochai, S., Schutte, K., Peters, P.W.M., 1991. Strain concentration factors for fibers and matrix in unidirectional composites. Compos. Sci. Technol. 41, 237–256.

Reedy Jr., E.D., 1984. Fiber stress in a cracked monolayer: comparison of shear-lag and 3D finite element predictions. J. Compos. Mater. 18, 595–607.

Ryvkin, M., Aboudi, J., 2007. The effect of a fiber loss in periodic composites. Int. J. Solids Struct. 44, 3497–3513.

Ryvkin, M., Nuller, B., 1997. Solution of quasi-periodic fracture problems by the representative cell method. Comp. Mech. 20, 145–149.

Sastry, A.M., Phoenix, S.L., 1993. Load redistribution near non-aligned fibre breaks in a two-dimensional unidirectional composite using break-influence superposition. J. Mater. Sci. Lett. 12, 1596–1599.

Sneddon, I.N., 1951. Fourier Transforms. McGraw Hill, New York.